

# **RECENT ERDC DEVELOPMENTS IN COMPUTATIONALLY MODELING CONCRETE UNDER HIGH RATE EVENTS<sup>1</sup>**

James O'Daniel

*US Army Engineer Research and Development Center, Vicksburg (MS), USA  
James.L.O'Daniel@usace.army.mil*

## **ABSTRACT**

Personnel of the US Army Engineer Research and Development Center (ERDC) have been performing a considerable amount of work in enhancing and developing numerical methods and constitutive models for simulating standard strength and higher strength fiber reinforced concrete. Methods currently under investigation include one based upon the Reproducing Kernel Particle Method (RKPM) and another using the Lattice Discrete Particle Method (LDPM). Developments in constitutive models include the generation of the Advanced Fundamental Concrete (AFC) model, based on improving the Holmquist-Johnson-Cook (HJC) model, and the adaptation of the Microplane Model to include the effects of fibers.

A set of experiments was performed where a fragment simulating projectile (FSP) penetrated several thicknesses of a fiber reinforced concrete (FRC) panel. Several of the methods and material models were used to simulate these tests, concentrating on various ways to model the FRC. The HJC model, the AFC model, and the Karagopian & Case Concrete Model from LS-DYNA were all inserted into a standard continuum finite element grid simulation. The Lattice Discrete Particle Method was also used in several forms, including one that homogenized the effects of the fibers into the constitutive model and another that explicitly modeled the fibers and discretely inserted their contribution into the vector constitutive equations only at specific locations where a fiber existed. Extensive characterization data has been developed for the FRC material examined in this study in the form of results from stress and strain path tests, fiber pullout experiments, and third point bending tests. Model parameters were generated against this data and then used for the high rate penetration simulations. Under investigation was how well these methods replicate the various possible mechanics found in the problem, ranging from projectile penetration and crater formation to complete perforation with a high residual velocity of the penetrator. Comparisons will be presented between the different methods and models and commentary given on each.

## **INTRODUCTION**

As fiber reinforced concrete (FRC) becomes used more frequently for structures that are, or can be, subjected to high rate penetration and explosive events, the ability to accurately simulate the response of those structures to these types of events becomes more important. Our interest involves the complete response of the structure under those loadings conditions, which possibly includes elastic, plastic, fragmentation, crushing, spall, and other failure types of behaviors in cementitious materials like FRC. FRC can easily be defined at multiple scales, and we refer to and investigate several of these, including, the macroscale (structural component level), the mesoscale (individual fiber and the surrounding concrete matrix), and the microscale (interface transition zone between the fiber and matrix and the components of the concrete matrix). Multiscale modeling involves the use of two or more of these scales and the interaction between them, transferring useful information from one to the other and back as necessary.

---

<sup>1</sup> Abstract approved for public release. Distribution is unlimited.

<b>Report Documentation Page</b>		<i>Form Approved OMB No. 0704-0188</i>
Public reporting burden for the collection of information is estimated to average 1 hour per response, including the time for reviewing instructions, searching existing data sources, gathering and maintaining the data needed, and completing and reviewing the collection of information. Send comments regarding this burden estimate or any other aspect of this collection of information, including suggestions for reducing this burden, to Washington Headquarters Services, Directorate for Information Operations and Reports, 1215 Jefferson Davis Highway, Suite 1204, Arlington VA 22202-4302. Respondents should be aware that notwithstanding any other provision of law, no person shall be subject to a penalty for failing to comply with a collection of information if it does not display a currently valid OMB control number.		
1. REPORT DATE <b>OCT 2010</b>	2. REPORT TYPE <b>N/A</b>	3. DATES COVERED <b>-</b>
4. TITLE AND SUBTITLE <b>Recent Erdc Developments In Computationally Modeling Concrete Under High Rate Events1</b>		5a. CONTRACT NUMBER
		5b. GRANT NUMBER
		5c. PROGRAM ELEMENT NUMBER
6. AUTHOR(S)		5d. PROJECT NUMBER
		5e. TASK NUMBER
		5f. WORK UNIT NUMBER
7. PERFORMING ORGANIZATION NAME(S) AND ADDRESS(ES) <b>US Army Engineer Research and Development Center, Vicksburg (MS), USA</b>		8. PERFORMING ORGANIZATION REPORT NUMBER
9. SPONSORING/MONITORING AGENCY NAME(S) AND ADDRESS(ES)		10. SPONSOR/MONITOR'S ACRONYM(S)
		11. SPONSOR/MONITOR'S REPORT NUMBER(S)
12. DISTRIBUTION/AVAILABILITY STATEMENT <b>Approved for public release, distribution unlimited</b>		
13. SUPPLEMENTARY NOTES <b>See also ADA550809. Military Aspects of Blast and Shock (MABS 21) Conference proceedings held on October 3-8, 2010. Approved for public release; U.S. Government or Federal Purpose Rights License., The original document contains color images.</b>		

14. ABSTRACT

Personnel of the US Army Engineer Research and Development Center (ERDC) have been performing a considerable amount of work in enhancing and developing numerical methods and constitutive models for simulating standard strength and higher strength fiber reinforced concrete. Methods currently under investigation include one based upon the Reproducing Kernel Particle Method (RKPM) and another using the Lattice Discrete Particle Method (LDPM). Developments in constitutive models include the generation of the Advanced Fundamental Concrete (AFC) model, based on improving the Holmquist-Johnson-Cook (HJC) model, and the adaptation of the Microplane Model to include the effects of fibers. A set of experiments was performed where a fragment simulating projectile (FSP) penetrated several thicknesses of a fiber reinforced concrete (FRC) panel. Several of the methods and material models were used to simulate these tests, concentrating on various ways to model the FRC. The HJC model, the AFC model, and the Karagopian & Case Concrete Model from LS-DYNA were all inserted into a standard continuum finite element grid simulation. The Lattice Discrete Particle Method was also used in several forms, including one that homogenized the effects of the fibers into the constitutive model and another that explicitly modeled the fibers and discretely inserted their contribution into the vector constitutive equations only at specific locations where a fiber existed. Extensive characterization data has been developed for the FRC material examined in this study in the form of results from stress and strain path tests, fiber pullout experiments, and third point bending tests. Model parameters were generated against this data and then used for the high rate penetration simulations. Under investigation was how well these methods replicate the various possible mechanics found in the problem, ranging from projectile penetration and crater formation to complete perforation with a high residual velocity of the penetrator. Comparisons will be presented between the different methods and models and commentary given on each.

15. SUBJECT TERMS

16. SECURITY CLASSIFICATION OF:			17. LIMITATION OF ABSTRACT	18. NUMBER OF PAGES	19a. NAME OF RESPONSIBLE PERSON
a. REPORT <b>unclassified</b>	b. ABSTRACT <b>unclassified</b>	c. THIS PAGE <b>unclassified</b>	<b>SAR</b>	<b>20</b>	

Research at ERDC encompasses the above scales ranging from developing better phenomenological models based at the macroscale, to explicitly modeling the constituents at the mesoscale, to looking at what is occurring at the microscale.

Phenomenological constitutive models have been used in finite element (FE) codes since their inception to simulate concrete. These models generally use empirically based results smeared into isotropic homogeneous behavior to capture the gross response of the concrete material. The Holmquist-Johnson-Cook (HJC) model [1] has been implemented into multiple codes, including EPIC [2] and LS-DYNA [3], and ERDC has used this material model to do extensive simulations in the blast and impact regimes. The Karagopian & Case Concrete Model [4] is a three-invariant model that uses three shear failure surfaces and includes damage and strain rate effects. While these two models are not new developments, the Army Fundamental Concrete (AFC) model [5] was developed to address several shortcomings of the HJC model, including the addition of the third invariant. The Microplane model [6-9] adds a pseudo-smaller scale by using constitutive relationships across multiple planes within an element. These planes do not physically represent any part of the actual material, but use vectors and bounding conditions on each plane, which allows anisotropic behavior to be captured. While those models improve the constitutive modeling capabilities of the codes, two programs are further developing overall modeling methods – instead of the traditional finite element method – to simulate FRC. The Reproducing Kernel Particle Method (RKPM) [10-13] is a meshfree method that inherently allows the domain to fragment, separate, and fail, as there is no connectivity between the constructs, i.e. no element to fail and/or erode to allow separation. While RKPM is based on continuum mechanics, the Lattice Discrete Particle Method (LDPM) [14-18] is a discrete model with similar traits to the planes in the Microplane model, performing the constitutive relations through planes between particles. Explicitly modeled fibers have been added to the method to enable mesoscale modeling of FRC. This type of approach will be used to model the interface transition zone (ITZ) between an individual fiber and the surrounding concrete matrix to capture the complicated relationship between them.

Penetration experiments were performed using a fragment simulating projectile (FSP) fired into FRC panels to examine their response. This will be the form of experiment to which each of the methods will be applied. Comparisons will be made quantitatively for the residual velocity in the FSP and qualitatively for the resulting damage to the panel. While there are similarities in the calculation of damage between several of the methods, the definition of damage to the FRC still has widely varying definitions, so each method/model will use its own damage definition, and that damage will be broadly compared and compared against the visual damage seen in the experiment. Most of the methods reported here are not in their final stage of development, and the current state of each will be used. Though they are considered mature, they are not yet perfected or finalized.

These simulations were performed in various codes as the methods were not contained within a single solver. The HJC and AFC models resided within the EPIC code. The K&C model implementation within LS-DYNA was used for this study. RKPM has only

been used within its research code to this point, but there are plans to implement it within other codes, such as EPIC, in the near future. The Microplane model for FRC has been inserted into a research version of EPIC, while LDPM is available within the MARS code. Significant effort will be put into moving these models and methods into production versions of codes.

Brief descriptions of the constitutive models and methods above are provided in the Numerical Methods section, as are the details on the comparative FSP penetration case. Some of the methods are still in the developmental stages, and results for the FSP penetration problem were not available at the time of writing. Available results are then discussed, including specific quantitative comparisons and general commentary on the methods used. Finally a brief summary is presented.

## NUMERICAL METHODS

### Phenomenological Models

The macroscale phenomenological constitutive models (HJC, AFC, and K&C) share the same basis in plasticity theory and have many similar traits. Material behavior is based around the separation of the hydrostatic and deviatoric behaviors for all three models. HJC and AFC explicitly calculate the pressure-volume relationship through the definition of crushing and locking points and using an equation to fit the remainder of the curve. This relation, otherwise called an equation of state, is defined by a set of points within the K&C model. A failure surface defines the limits on the deviatoric behavior, and while the HJC model is constrained by only using the first two invariants, the AFC and K&C improve upon the modeling by implementing the third invariant, allowing the compression and extension failure surfaces to be defined independently. A basic description of that model is included here.

### AFC Model

Adley, et. al. [5, 19] provide a total description of the AFC model and examples of its application. Our constitutive model is built around a three-invariant plasticity model. The model simulates irreversible hydrostatic crushing, material yielding, plastic flow, and damage. The model has a non-linear pressure volume relationship and a linear shear relationship (constant G). The model also includes strain-rate effects for the failure surface (increasing shear strength with increasing strain rates). As with most of the simple constitutive models for concrete, our model separates the hydrostatic response from the deviatoric response. Thus the hydrostatic and deviatoric responses are independently calculated without providing any coupling between the two (no volumetric strain due to pure deviatoric loading can develop).

Hydrostatic behavior of our model includes a non-linear bulk modulus and irreversible volumetric crushing that contributes to material damage. More specifically the compressive hydrostatic behavior can be separated into three distinct regions: an initial elastic zone, an irreversible crushing response, and an elastic locking region. This

behavior is similar to that modeled by Holmquist, Johnson, and Cook [1]. Furthermore, the model treats initial loading, unloading, and reloading differently.

The initial elastic zone for the model only occurs for volume strains below the crushing volume strain value ( $U_{crush}$ ). Initial loading, unloading, and reloading in the elastic zone all follow linear elastic behavior defined by the elastic bulk modulus ( $K_e = P_{crush}/U_{crush}$ ), where  $P_{crush}$  is the maximum attainable pressure for the initial elastic zone. The end of this region is defined when the air voids begin to be crushed and nonlinear behavior results.

The irreversible crushing response occurs for all material in which the volume strain has exceeded the crushing volume strain value ( $U_{crush}$ ) but has not exceeded the locking volume strain value ( $U_{lock}$ ). The crushing region is defined by letting the origin of the crushing response coincide with the point in pressure-volume space ( $P_{crush}, \mu_{crush}$ ). Hence, that same point also coincides with the ending of the initial elastic zone. Within this second region all the air voids are compressed, generating plastic volumetric strain within the concrete, until no more voids are present and the concrete locks and enters into the third region of hydrostatic behavior. Unloading within the second region is interpolated from the adjacent regions. The locking region is characterized by permanent volume compaction and follows the third order polynomial equation:

$$P = K_1\mu + K_2\mu^2 + K_3\mu^3 \quad (1)$$

where  $K_1, K_2, K_3$  are input parameters,  $P$  is the mean normal stress (pressure), and  $\mu$  is a measure of volumetric strain. It should be noted that this equation uses the soil mechanics sign convention (compression > 0), which means that the pressure ( $P$ ) as computed by the previous equation is equal to the first invariant of the stress tensor ( $I_1$ ) multiplied by -1, i.e.  $I_1 = -P$ . In the crushing region unloading and reloading are non-linear, with the bulk modulus varying linearly between  $K_e$  and  $K_{lock}$  as  $\mu$  varies between  $U_{crush}$  and  $U_{lock}$ . However, since the change in  $\mu$  during a typical unload-reload cycle in the crush zone is generally only a small percentage of the value of ( $U_{lock} - U_{crush}$ ), the response in most cases is nearly linear.

The linear elastic locking region in the model is defined by a locking bulk modulus ( $K_{lock}$ ) and occurs for volume strains above the locking value for volumetric strain ( $U_{lock}$ ). Unloading and reloading in the locking region are purely linear elastic and also follow the locking bulk modulus ( $K_{lock}$ ).

The tensile hydrostatic behavior of the model is always defined by linear elastic behavior and follows a bulk modulus that is between the elastic bulk modulus ( $K_e$ ) and the locking bulk modulus ( $K_{lock}$ ), depending on the level of permanent volumetric crushing. For example, the tensile hydrostatic behavior follows the elastic bulk modulus ( $K_e$ ) for any material in which volume strains have not exceeded the initial crushing volume strain value ( $U_{crush}$ ). However, if the material has exceeded  $U_{crush}$ , the tensile hydrostatic behavior follows an elastic bulk modulus that is greater than or equal to  $K_e$ , and less than or equal to  $K_{lock}$ . Since the change in  $\mu$  during a typical unload-reload cycle in the tensile zone is generally only a small percentage of the value of ( $U_{lock} - U_{crush}$ ), the response in most cases is nearly linear.

Next we will describe the deviatoric behavior of the model, which includes material yielding plastic flow and damage. Notice that an engineering mechanics sign convention has been used, hence the mean normal stress (pressure) values less than zero denote compression. The compression yield surface is represented by the following two equations, depending on whether the hydrostatic component of the stress state is in compression or tension.

For stress states where the first invariant of the stress tensor ( $I_1$ ) is less than or equal to zero (indicative of compression), the failure surface is expressed as:

$$S_Y = (C_1 - (C_2 + (C_1 - C_2)D)e^{A_n I_1} - C_4 I_1)(1 + C_3 \ln(\dot{\varepsilon}_n)) \quad (2)$$

where  $C_1$ ,  $C_2$ ,  $C_3$ ,  $C_4$ , and  $A_n$  are constants that are greater than or equal to zero,  $D$  is a damage parameter that varies between 0 and 1, and  $\dot{\varepsilon}_n$  is an effective deviatoric strain rate which is normalized to a reference rate that is provided as input. It should also be noted that the values of  $C_1$  and  $C_2$  must satisfy the constraint  $C_1 \geq C_2$ .

For stress states where the first invariant of the stress tensor ( $I_1$ ) is greater than zero (indicative of tension), the failure surface is expressed as:

$$S_Y = (C_1 - (C_2 + (C_1 - C_2)D))(1 + C_3 \ln(\dot{\varepsilon}_n))(T_{\max} - I_1)/T_{\max} \quad (3)$$

where  $T_{\max}$  is the maximum allowable tensile pressure, and the value of  $S_y$  is restricted to values that are greater than or equal to zero.

The third-invariant dependence of the failure surface is computed using the Lode angle. For example, a discrete extension failure surface value is computed by first computing the value of the compression failure surface at the stress state of interest, and then multiplying the compression failure surface value by a factor that is a function of the third invariant of the deviatoric stress tensor. Specifically, the Lode angle is computed, and then the value of the aforementioned factor is computed by evaluating either the William-Warnke Lode function [5] or the Gudehus Lode function [5].

As stated previously, our constitutive model also accounts for material damage that develops during the course of stress/strain loading histories. This material damage effectively provides a reduced failure surface due to excessive plastic shear strain as well as excessive hydrostatic crushing. The value of material damage is quantified using a scalar damage parameter ( $D$ ) that is computed by evaluating the damage equation:

$$D = \sum \left( \frac{\Delta \varepsilon_p}{-I_1 D_1} + \frac{\Delta \mu_p}{1.5 U_{\text{lock}}} \right) \quad (4)$$

where  $D_1$  is an input parameter which is greater than zero, values of the expression  $(-I_1 D_1)$  are restricted to values greater than 0.01,  $\Delta \varepsilon_p$  is an increment in the effective deviatoric plastic strain,  $\Delta \mu_p$  is an increment of volumetric plastic strain, and  $U_{\text{lock}}$  is the locking volumetric strain value previously described. Notice that the material damage

parameter (D) is included in calculation of the failure surface as shown above in equations 2 and 3.

### **Reproducing Kernel Particle Method**

RKPM is a meshfree method formulated based on a reproducing kernel approximation. In this method, a correction function is introduced in the kernel approximation so that the arbitrary order of consistency, arbitrary order of smoothness, controllable locality, and adaptive model refinement can be achieved and implemented with a relative ease compared to the conventional mesh based finite element method. They introduced a correction function in the kernel of integral transformation to impose reproducing conditions. Adding the correction function in the kernel significantly enhances the solution accuracy when compared to prior meshless formulations. The method satisfies the reproduction conditions, and therefore, exactly reproduces polynomials. This method provides a general formulation for the construction of shape functions for meshless computation. Using specific discretization of the reproducing equation, other meshless methods can be recovered. The theory of wavelet analysis has been combined in RKPM by introducing the scaling function as the kernel function and successfully applied RKPM to multiple scale analysis.

In the Lagrangian formulation, the basis functions, moment matrix and kernel functions are evaluated in the undeformed configuration. However, Lagrangian formulation breaks down when modeling the penetration and fragmentation processes in which the deformation gradient loses positive definiteness when there exists new free surface formation or free surface closure in the damage evolution processes. To address this difficulty, a semi-Lagrangian reproducing kernel approach was added.

In semi-Lagrangian discretization, the discrete meshfree particles follow the material motion; however, the kernel is evaluated using a distance measured in the deformed configuration. Under this definition of distance measure, the material particles covered under the kernel support are allowed to vary during material deformation. ERDC has teamed with J.S. Chen (UCLA) to advance RKPM, adapt its ability to model FRC, and develop a multiscale approach to these types of materials. Nodal stability formulations have been developed that greatly enhance the accuracy and add stability over direct nodal integration schemes. Methods have been developed and improved in the areas of combining and attaching RKPM and FEM domains within a single problem, automatic adaptive refinement of the RKPM domain, the semi-lagrangian formulation briefly described above, and combining the RKPM method with the appropriate constitutive models for concrete materials.

Enabling RKPM to model FRC was accomplished through the implementation of the AFC model into the research code. This allowed a better constitutive representation of the concrete material while using the RKPM methodology. Further work has included subscale informed damage (multiscale modeling). The damage is determined through subscale RKPM models that can capture the cracking behavior of the FRC and transmit that information back to the macroscale as a change in the damage parameter. Various

types of the damage parameter are being investigated, from a simple, single scalar parameter to using different damage parameters in shear and tension to a complex damage tensor. Figure 1 shows a possible change in the yield surface as damage scalars in shear,  $D_s$ , and tension,  $D_t$ , are applied separately to reduce the extent of the surface.

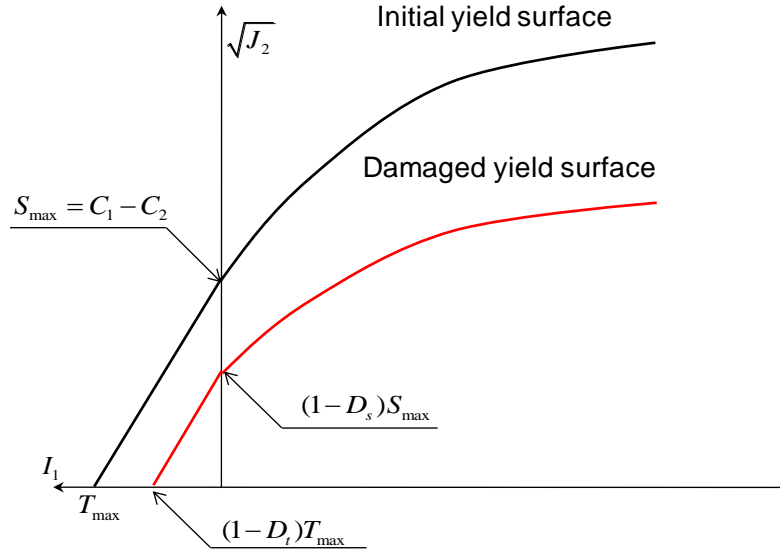


Figure 1: Reduction of the yield surface within the RKPM/AFC Model

### **Microplane Model for FRC**

Significant development of the Microplane model has been done over the last 20 years by Bazant, and the current ERDC effort is to extend the microplane formulation to be applied to FRC materials. The basic idea of the microplane concept is to formulate the constitutive equations between single scalar- and vector-valued stress-strain components on individual microplanes. Thus, the microplane parameters obtain a physical meaning and interpretation. The microplane theory is summarized in schematic form in Figure 2. The three main steps of the microplane model are illustrated. The first step is the projection part. Here a kinematic constraint is applied in order to relate the macroscopic strain tensor to its microplane counterparts. The kinematic constraint assumes that the microplane strains are equivalent to the projected macroscopic strain tensor, opposite to a static constraint, where the stresses are projected. The microplane strains can be derived as projections of the overall strain tensor, which corresponds to the symmetric part of the displacement gradient in the geometrically linear case. The second step describes the definition of constitutive laws on the microplane level. These constitutive equations are formulated between single stress and strain components on individual microplanes and have, in most versions up to now, been assumed to be unidirectional. The last step of microplane modeling relates to the homogenization process on the material point level to derive the overall response. This homogenization process is based on the principle of energy equivalence. Thereby, in former microplane formulations, the overall response was derived through a homogenization process based on the principle of virtual work.

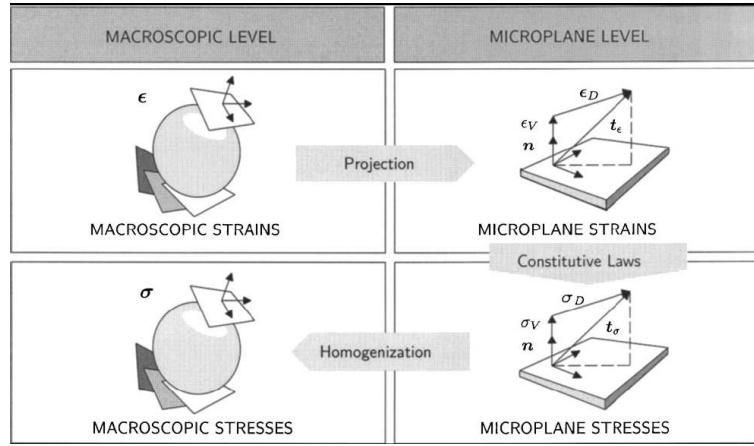


Figure 2: Macroscopic-Microscopic process of Microplane Model

Current efforts address the bounding curves that exist for each microplane. Fibers are not explicitly modeled, but their behavior is captured through modification of the bounding curves that defined the extent of variables within the constitutive behavior. A challenge is that, unlike normal concrete, the fiber reinforced concrete resists tension and shear up to extremely large tensile strain, which requires capturing the transition to constrained fracture. The basic idea for extending the microplane model to FRC was simply to add fiber resistance to the tensile resistance of the individual microplanes of various orientations. Fiber resistance must be modified for fiber slip within concrete. Breakage of fibers as well as their pullout from the crack faces must be captured. Bounding curves of the microplane model become surfaces that vary with percent volume of fibers. An example surface is shown in Figure 3, where the deviatoric stress-strain ( $\sigma_D$ - $\epsilon_D$ ) relation changes with an increase in the percent volume of fibers ( $V_f$ ).

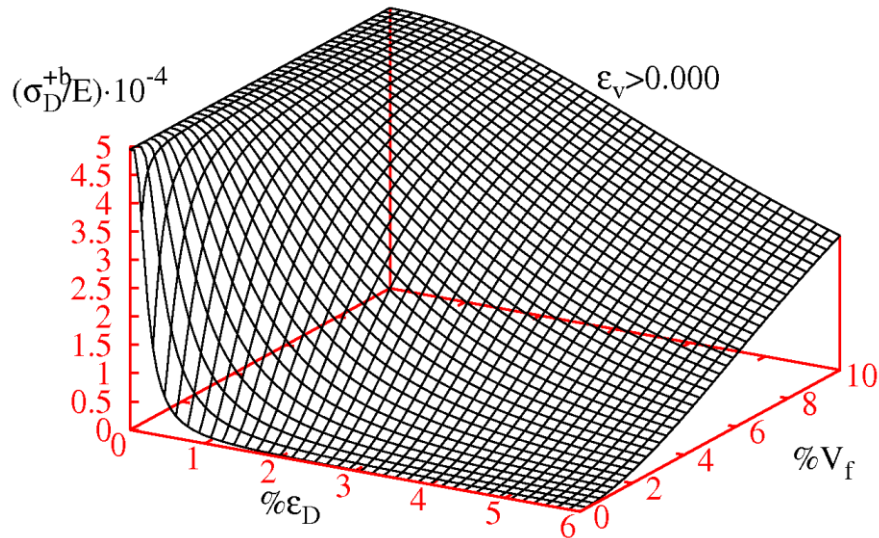


Figure 3: Deviatoric Stress-Strain Bounding Surface in Microplane Model for FRC

Recent improvements done by Bazant include: employing a volumetric-deviatoric coupling in stress tensor calculation, using a simpler, more explicit transition from volumetric-deviatoric split formulation to a no split formulation under uniaxial tension, new normal boundary including fiber effects, new deviatoric boundaries as functions of volumetric strain and including fiber effects, and implementing an energy dissipation calculation to ensure realistic, positive dissipation. Further work includes: investigation of rate effects on this FRC model, calibration/fitting of the model to determine extent of effectiveness of the model, and validation of the model against impact and blast high rate problems.

## Lattice Discrete Particle Method

LDPM simulates concrete mesostructure by taking into account only the coarse aggregate pieces, typically with characteristic size greater than 5 mm. The mesostructure is constructed through the following steps. 1) The coarse aggregate pieces, whose shapes are assumed to be spherical, are introduced into the concrete volume by a try-and-reject random procedure. 2) Zero-radius aggregate pieces (nodes) are randomly distributed over the external surfaces. 3) A three-dimensional domain tessellation, based on the Delaunaytetrahedralization of the generated aggregate centers, creates a system of cells interacting through triangular facets, which can be represented in a two-dimensional sketch by straight line segments (Fig. 4).

A vectorial constitutive law, very similar to the constitutive law applied to each microplane, governing the behavior of the model is imposed at the centroid of the projection of each single facet (contact point) onto a plane orthogonal to the straight line connecting the particle centers (edges of the tetrahedralization). The projections are used

instead of the facets themselves to ensure that the shear interaction between adjacent particles does not depend on the shear orientation. The straight lines connecting the particle centers define the lattice system. Rigid body kinematics describes the displacement field along the lattice struts and the displacement jump at the contact point.

LDPM is extended to include the effects of randomly dispersed fibers in order to simulate the behavior of fiber reinforced concrete (FRC). During the pre-processing phase, each individual fiber is inserted into the specimen volume. Fiber positions and orientations are randomly generated, and the intersections between fibers and LDPM facets are detected. By assuming a parallel coupling between the fibers and the concrete matrix, stresses are computed. The concrete stress components are computed

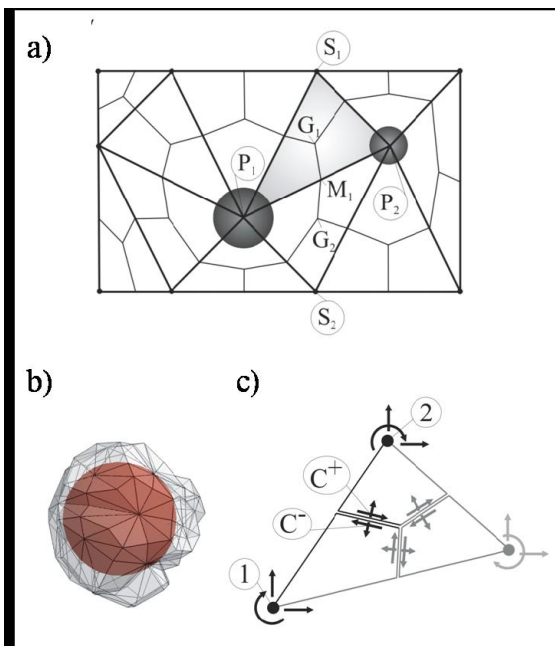


Figure 4: a) Mesostructure tessellation. b) Three-dimensional discrete particle. c) Definition of nodal degrees of freedom and contact facets in two dimensions.

according to the basic LDPM constitutive law described above. The fiber contribution to the crack bridging force is computed according to a micro-structural fiber-matrix interaction model developed by Lin, et al. [20].

Fragment Simulating Penetrator (FSP) experiments have been carried out at ERDC, and simulations have been performed using the Lattice Discrete Particle Method. Simulations of steel projectile impacts into fiber reinforced concrete (FRC) slabs at various impact velocities are presented. The simulated slabs were 304.8 mm squares with thicknesses ( $t$ ) varying from 12.7 mm up to 76.2mm. Impact velocities of up to 450 m/sec and three different fiber volume fractions (Vf) - 0%, 2%, and 3% were modeled in the simulations. The ballistic limit (the highest strike velocity associated with zero residual velocity) increased for increasing Vf. The 3% Vf simulations show that an increase in fiber content does not necessarily correspond to a significant increase in the ballistic limit. Finally, the effect of the fibers becomes less significant for higher striking velocities. This is due to the fact that at very high striking velocities, the penetration phenomenon is governed more by the mass of the system and the confined compressive resistance, than by tensile fracturing behavior, which is significantly influenced by the presence of the fibers. Several methods of attaching the fibers to the matrix of concrete particles have been attempted, including the original method where the fiber elements were slaved to the master concrete particles. The behavior was not captured well in this version, so an improved coupling was developed where a contribution from the fiber was applied to each facet that it crossed; so when a facet “cracked” and separated, the tensile behavior would have the response of the fiber added to resist the crack opening. Current efforts include calibration and validation of the LDPM with fibers method against the ERDC experimental results.

## EXPERIMENT DESCRIPTION

The small arms ballistic testing facility at the ERDC consists of an underground ballistic range with an outside support building. The outside support building houses a cartridge preparation area that includes the proper equipment to hand-load numerous varieties of cartridges. Figure 5 shows the apparatus used to fire the projectiles.

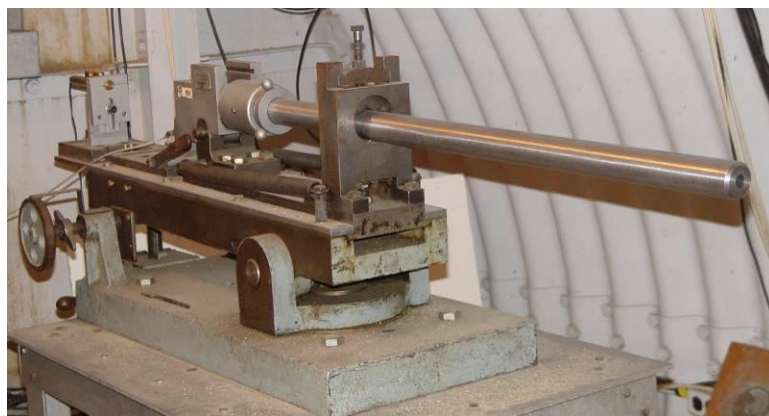


Figure 5: Modern Bond Universal Small-Arms Receiver Used to Fire the Projectiles

Projectile velocity measurements were made using a pair of Oehler Research, Inc. model 35P proof chronographs, each connected to two Oehler model 55 light screens. The light screens attached to each chronograph were positioned 0.91 m apart to measure fragment velocities. To measure entrance and exit (residual) velocities for each experiment, pairs of chronograph screens (Figure 6) were positioned so that each pair's midpoint was located approximately 1.68 m ahead of and 1.37 m behind the test specimens.

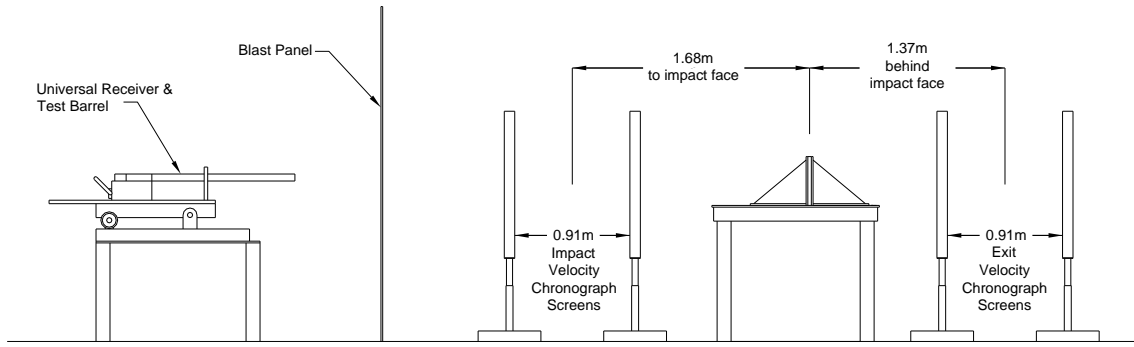


Figure 6: Schematic of Ballistic Penetration Test

Experiments were conducted to measure the FRC's resistance to ballistic projectile penetration. Slabs tested were of uniform 304.8 mm by 304.8 mm size with an approximate thickness of 50.8 mm. Posttest qualitative observations were also made by visual inspection of the slab and witness panel. These observations were documented with digital photography to capture the effects of material fragments on the exit or "safe" side of the panels.

Each FSP was a 0.50 caliber projectile, approximately 14.7 mm long, with a diameter of about 12.7 mm, and a weight of 207 grains (13.41 g). The FSP was designed to simulate a typical metal fragment from a detonating cased munition. The nominal projected impact velocity was 1,112 m/sec, with the actual impact velocity being measured by the FSP breaking the chronograph planes before striking the target. Impact velocities were as close as the variance between tests allowed. Those measured velocities were used as the input velocities in the simulations. An example of FRC penetration is shown in Figure 7.

The particular FRC used in the experiments is called Cor-Tuf [21], developed at ERDC. Cor-Tuf exhibits a compressive strength of approximately 220 MPa and contains approximately 3.6% by volume steel fibers. The fibers are approximately 30-mm long, have a diameter of approximately 0.55 mm, and are hooked at each end. The tensile strength for the steel fibers is reported by the manufacturer to be 1,100 MPa. Each FSP is made from 4340 steel, and textbook [22] values are used (including density of 7,833.4 kg/m<sup>3</sup>, a yield strength of 1,482.4 MPa, an ultimate strength of 1,578.9 MPa, a failure strain of 16.0%, and a Young's Modulus of 207,000 MPa) in the simulations as coupon tests are not performed for the materials. Steel is simulated with a Johnson-Cook material [23] model.

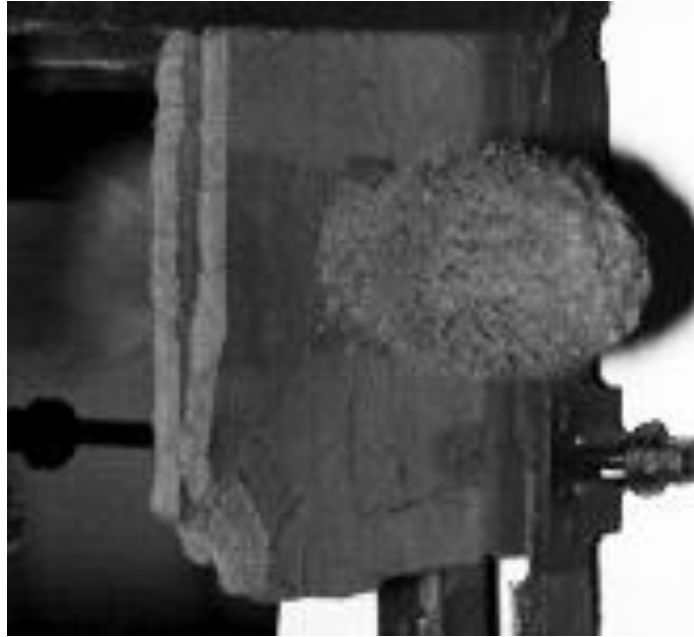


Figure 7: Resulting debris from FSP perforation to concrete panel

## NUMERICAL MODEL

As the codes were not all at the point in their development to be able to simulate the penetration problem just described, only the phenomenological models and the LDPM were used to compare results for the penetration of the FSP through a 50.8 mm thick FRC panel. The same numerical model base discretization was used for the HJC and AFC models in EPIC and the K&C model in LS-DYNA. A mesh containing approximately 500,000 eight-noded hexahedral (hex) elements (Figure 8a) was generated and used directly within LS-DYNA. EPIC converts each hex to 24 tetrahedral (tets) elements, so the discretization for those simulations was significantly higher. The mesh contained a higher concentration of elements within the center (the impact location) and was graded linearly to larger elements at the outside boundaries. The hex elements started with a nominal size of 1.0 mm in each direction. The FSP contained approximately 20,000 hex elements (Figure 8b) and was also changed to tets within the EPIC simulations. An LDPM model using the same FSP discretization and having a Cor-Tuf panel containing 527,000 particles was developed.

## RESULTS

Complete perforation of the Cor-Tuf panel was achieved during the experiment, with an impact velocity of 1,084.2 m/sec and a residual penetrator velocity measured at 85.6 m/sec. Views of the impact and exit sides of the slab are shown in Figure 9. Spall diameter was larger on the exit side, surrounding an exit hole that had a diameter of about 28.0 mm. A large number of fibers can be seen extending out from the damaged concrete matrix. While the exact deformed FSP was not gathered and documented for each experiment performed, the typical deformation seen in these experiments is shown in Figure 10.

Results for the K&C model were inconclusive, as the behavior was deemed to be nonrealistic, and an extensive amount of research would have been required to determine the cause of the problems. Properties for the Cor-Tuf were generated by LS-DYNA from the input compressive strength. This strength is outside the typical values used and outside the range of behavior for which the K&C model has been validated. Further investigation of the problem was outside the scope of this work.

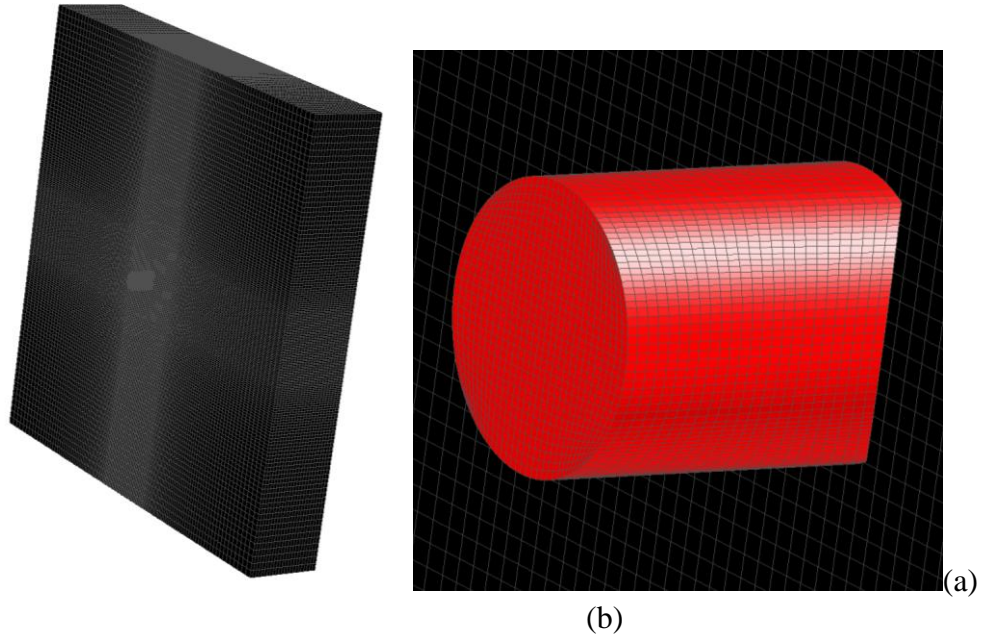


Figure 8: Discretization of Cor-Tuf Panel (a) and FSP (b)

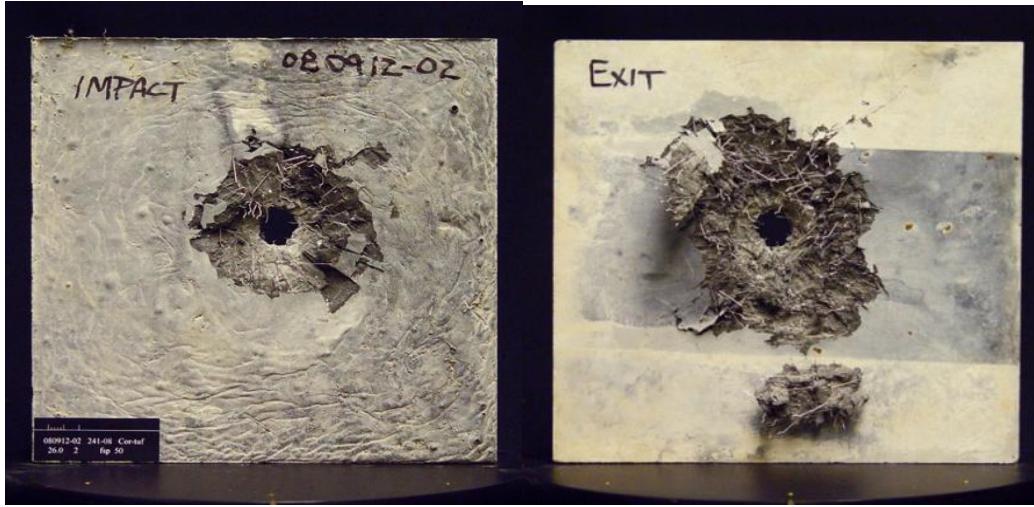


Figure 9: Impact and Exit Damage to 50.8 mm Cor-Tuf Panel



Table 1: FSP Residual Velocity

	<i>Velocity (m/sec)</i>
<i>Experiment</i>	<b>85.6</b>
<i>HJC</i>	<b>141.1</b>
<i>AFC</i>	<b>98.2</b>
<i>LDPM</i>	<b>88.7</b>

Figure 10: Example of deformed FSP

The remaining simulations of this experiment showed very similar deformation of the FSP, with the mushrooming of the impact tip. Table 1 contains the experimental and calculated residual velocities of the FSP. The AFC and LDPM cases are very close to the measured velocity, and the HJC calculated an exit velocity that was too high, but still significantly lower than the impact velocity. Post penetration views of the exit face of the Cor-Tuf panel for the HJC and AFC (at early time) are shown in Figure 11, plotting the damage parameter for each material model. Large vertical and horizontal cracks appear in the HJC results, while the AFC has very similar damage as was seen in the experiment. A 19.7 diameter hole is generated by the HJC model, while a 22.0 mm hole is generated when the AFC model was used.

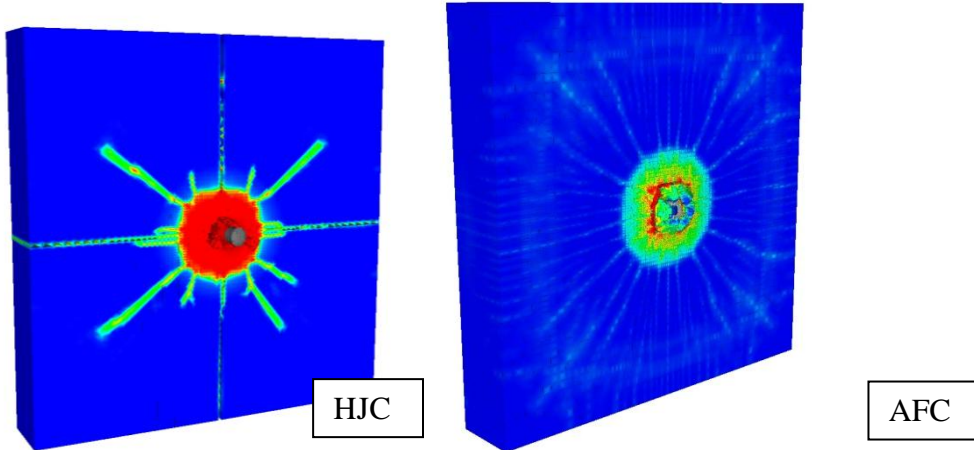


Figure 11: Exit side damage and FSP post-penetration for HJC and AFC models

Similar damage is seen when the LDPM is used to model the Cor-Tuf panel (Figure 12). The penetration hole is larger with a mean diameter of ~30.0 mm and there is more damage through the thickness. Further methods of modeling the fiber-matrix interaction are under investigation to better capture the behavior.

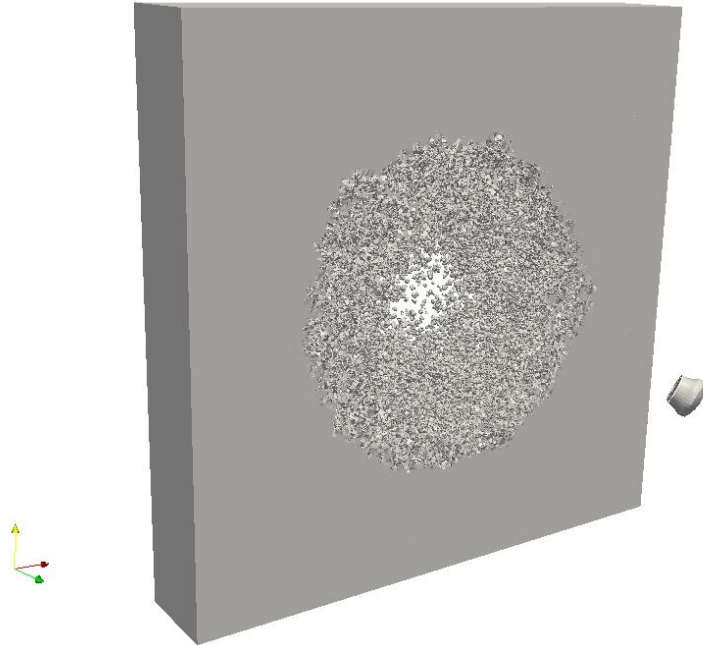


Figure 12: LDPM Penetration of Cor-Tuf Panel

Preliminary results from an RKPM/AFC simulation showing penetration of the FSP through a Cor-Tuf Panel are shown in Figure 13. At the early times shown, the damage (depicted in red) is trending in the correct amounts and locations across the section and is concentrated in the correct areas across the exit face. Significant work has been completed to allow subscale informed damage within the RKPM framework, and a good portion of the remaining work involves implementation of this method into production level codes (such as EPIC).

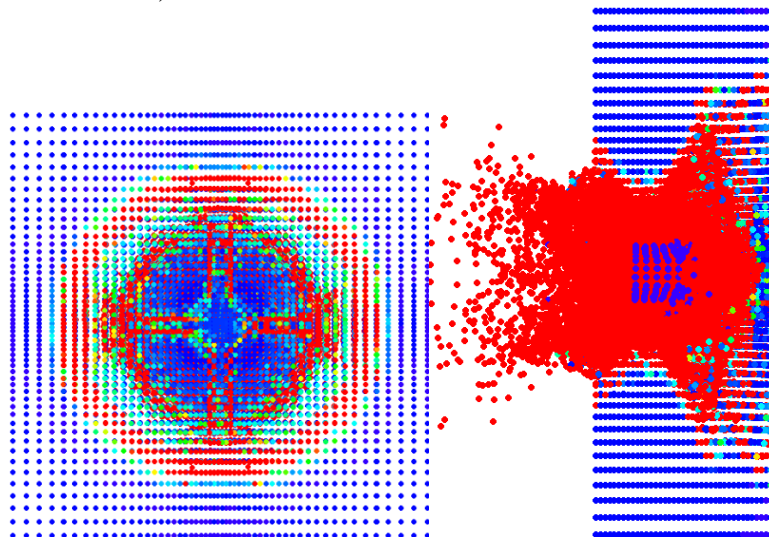


Figure 13: FSP penetration of a Cor-Tuf Panel, exit and side views

The Microplane Model for FRC (M4f) has been implemented into a research version of EPIC, and preliminary calculations have been performed using a projectile penetration case that has often been used as a baseline case for calibration. Efforts included the

addition of tensile artificial viscosity, generation of material parameters, and an examination of the effect of the number of microplanes used within each element. Figure 14 shows the results from an axial stress-strain plot when the number of planes varied from 21 to 61 planes. While computational time was increased, the pre-peak behavior was almost identical, and there wasn't a large difference in the post-peak behavior, considering that behavior is unstable.

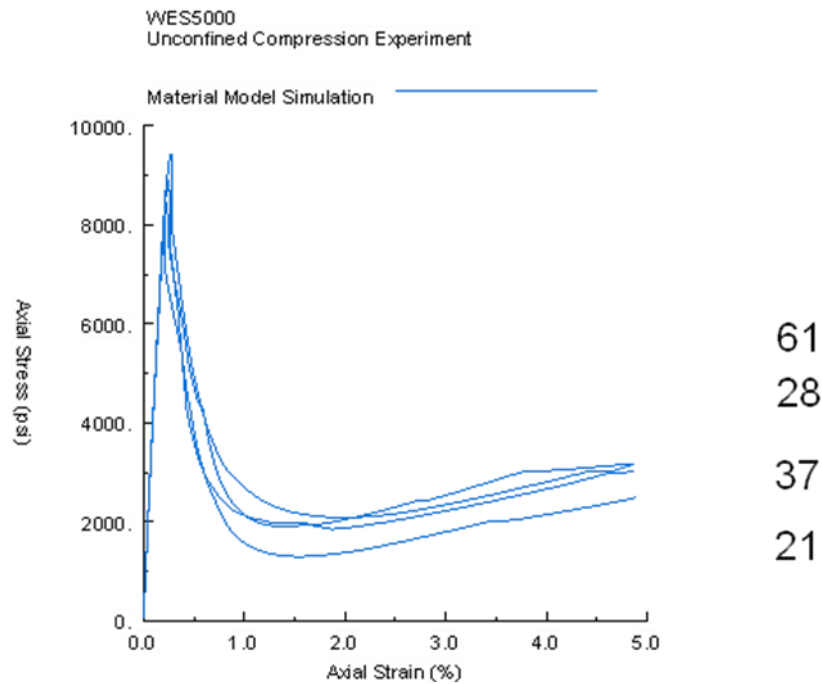


Figure 14: Multiple numbers of Microplanes for Stress-strain behavior

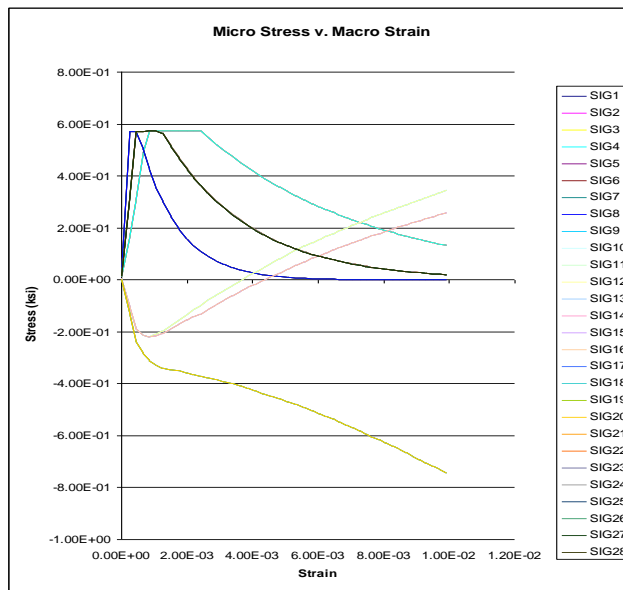


Figure 15: Stress-strain behavior on different microplanes in an element

An interesting part of the Microplane model is that the behavior on the different planes can be significantly different, as is shown in Figure 15, which displays the stress-strain behavior on the 28 different planes within a single element. Some overlap occurred, but a wide variation in the behavior can be seen. M4f exhibited good results considering the preliminary nature of its current implementation within EPIC. These contribute to the overall response of the element.

An example penetration is shown in Figure 16, plotting the plastic strain in the target FRC panel. General damaged volume is consistent with experimental data and similar in nature to other numerical results for this type of penetration and panel thickness.

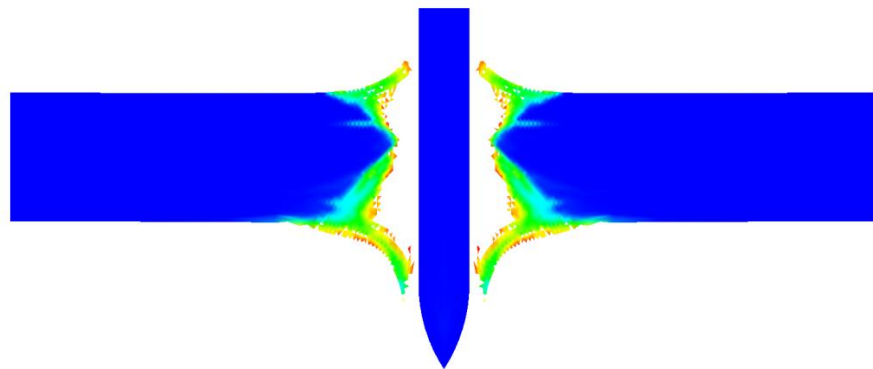


Figure 16: Penetration of FRC modeled with M4f

## SUMMARY

ERDC/GSL is involved in a considerable amount of research to develop computational methods and constitutive models that will more accurately simulate the response of FRC to high rate loadings. While most of these efforts are in progress, significant steps have been achieved for both phenomenologically modeling FRC and for multiscale modeling efforts. All of the current ERDC efforts (AFC, RKPM, LDPM, and Microplane) have shown promising results toward the simulation of FRC and being able to capture its behavior when subjected to high rate loading. The macroscopic AFC model is showing very good results while still allowing for relatively fast simulation speeds. The Microplane model has previously shown good results for impact and blast simulations, and the extension of the model to simulate FRC initially shows promise. Examination of the behavior at multiple scales with the RKPM and LDPM methods will allow us to examine detailed and precise behavior, investigating specific smaller scale behavior, which should generate more accurate macroscopic estimates of damage.

## ACKNOWLEDGEMENT

Permission to publish was granted by Director, Geotechnical and Structures Laboratory. All calculations were performed on Department of Defense Supercomputer Resource Center high performance computers. Numerous people contributed to the work described in this paper, including Dr. Kent Danielson, Dr. Andy Frank, Dr. Mark Adley, Dr. Beverly DiPaolo, Dr. Tom Slawson, and Nick Boone of ERDC; Dr. Daniele Pelessone of ES3; Prof. Zdenek Bazant of Northwestern Univ. and his team; Prof. J.S. Chen of UCLA and his team; and Prof. Gianluca Cusatis and his team from Rensselaer Polytechnic Institute.

## REFERENCES

- [1] Holmquist, T.J., Johnson, G.R., and Cook, W.H., "A computational constitutive model for concrete subjected to large strains, high strain rates and high pressures". Fourteenth International Symposium on Ballistics, Quebec City, Canada, September 1993.
- [2] Johnson, G.R., Beissel, S.R., Gerlach, C.A., Stryk, R.A., Holmquist, T.J., Johnson, A.A., Ray, S.E., and Arata, J.J., "User Instructions for the 2006 Version of the EPIC Code", Final Report, Contract DAAD19-03-D-0001, U.S. Army Research Laboratory, 2006.
- [3] LS-DYNA, user's manual, version 971\_R3, Livermore Software Technology Corporation, 2008.
- [4] Malvar, L.J., Crawford, J.E., Wesevich, J.W., Simons, D., A plasticity concrete material model for DYNA3D, International Journal of Impact Engineering, Volume 19, Issues 9-10, October-November Pages 847-873, 1997.
- [5] Adley, M.D., Frank, A.O., Danielson, K.T., Akers, S.A., and O'Daniel, J.L., "The Army Fundamental Concrete (AFC) Model", ERDC/GSL TR-10-XX [Forthcoming].
- [6] Bažant, Z.P., Caner, F.C., Carol, I., Adley, M.D., and Akers, S.A. "Microplane model M4 for concrete: I. Formulation with work-conjugate deviatoric stress." J. of Engrg. Mechanics ASCE 126 (9), 944-953, 2000.
- [7] Caner, F.C., and Bažant, Z.P. "Microplane model M4 for concrete: II. Algorithm and Calibration." J. of Engrg. Mechanics ASCE 126 (9), 954-961, 2000.
- [8] Bažant, Z.P., Caner, F.C., Adley, M.D., and Akers, S.A. "Fracturing rate effect and creep in microplane model for dynamics." J. of Engr. Mechanics ASCE 126 (9) 962-970, 2000.
- [9] Bažant, Z.P., Adley, M.D., Carol, I., Jirasek, M., Akers, S.A., Rohani, B., Cargile, J.D., and Caner, F.C. "Large-strain generalization of microplane model for concrete and application." J. of Engr. Mechanics ASCE 126 (9), 971-980, 2000.

- [10] Liu, W.K. , Jun, S. , Li, S. , Adee, J., and Belytschko, T., Reproducing Kernel Particle Methods for structural dynamics, *Int. J. Numer. Methods Engrg.* 38 1655-1679, 1995.
- [11] Liu, W.K. , Jun, S., and Zhang, Y.F., Reproducing Kernel Particle Method, *Int. J. Numer. Methods Fluids* 20 1081-1106, 1995.
- [12] Chen, J. S., Pan, C., Wu, C. T., and Liu, W. K., "Reproducing Kernel Particle Methods for Large Deformation Analysis of Nonlinear Structures," *Comput. Meth. Appl. Mech. Engng.* 139, 195-229, 1996.
- [13] Chen, J. S., Wu, C. T., Yoon, S., and You, Y., "A Stabilized Conforming Nodal Integration for Galerkin Meshfree Methods," *International Journal for Numerical Methods in Engineering*, Vol. 50, pp. 435-466, 2001.
- [14] Cusatis, G., Bazant, Z. P. and Cedolin, L., Confinement-shear lattice model for concrete damage in tension and compression: I. Theory. *J. of Engrg. Mech. (ASCE)*, 129(12):1439-1448, 2003.
- [15] Cusatis, G., Bazant, Z. P. and Cedolin, L., Confinement-shear lattice model for concrete damage in tension and compression: II. Computation and validation. *J. of Engrg. Mech. (ASCE)*, 129(12):1449-1458, 2003.
- [16] Cusatis, G., Bazant, Z. P. and Cedolin, L., Confinement-shear lattice model for fracture propagation in concrete. *Comput. Methods Appl. Mech. Engrg.*, 195:7154-7171, 2006.
- [17] Cusatis, G. and Cedolin, L., Two-scale analysis of concrete fracturing behavior. *Engng. Fracture Mech.*, 74:3-17, 2006.
- [18] Cusatis, G., Schauffert, E. A., Pelessone, D., O'Daniel, J.L., Marangi, P., Stacchini, M., Savoia, M. "Lattice Discrete Particle Model for Fiber Reinforced Concrete (LDPM-F) with Application to the Numerical Simulation of Armoring Systems", Computational Modeling of Concrete Structures (EURO-C), 15-18 March 2010.
- [19] Adley, M.D., Frank, A.O., Danielson, K.T., Akers, S.A., and O'Daniel, J.L., "The Virtual Penetration Laboratory: New Developments for Projectile Penetration in Concrete", *Computers and Concrete*, v 7, n 2, April 2010.
- [20] Lin, Z., Kanda, T. and Li, V. C., "On interface characterization and performance of fiber-reinforced cementitious composites". *Concr Sci Engng.*, 1:173-184, 1999.
- [21] Williams, E.M., Graham, S.S., Reed, P.A., and Rushing, T.S., "Laboratory Characterization of Cor-Tuf Concrete With and Without Steel Fibers", ERDC/GSL TR-09-00, May 2009.

[22] Harvey, P.D. (1982), Engineering Properties of Steel, American Society for Metals.

[23] Johnson G.R. and Cook, W.H., “A constitutive model and data for metals subjected to large strains, high strain rates, and high temperatures”. Seventh International Symposium on Ballistics, The Hague, The Netherlands, 1983.